PHILOSOPHICAL TRANSACTIONS OF THE ROYAL SOCIETY A

Phil. Trans. R. Soc. A (2011) **369**, 1412–1427
doi:10.1098/rsta.2010.0359

Drag reduction by riblets

By Ricardo García-Mayoral and Javier Jiménez*

School of Aeronautics, Universidad Politécnica de Madrid, 28040 Madrid, Spain

The interaction of the overlying turbulent flow with riblets, and its impact on their drag reduction properties are analysed. In the so-called viscous regime of vanishing riblet spacing, the drag reduction is proportional to the riblet size, but for larger riblets the proportionality breaks down, and the drag reduction eventually becomes an increase. It is found that the groove cross section A_g^+ is a better characterization of this breakdown than the riblet spacing, with an optimum $A_g^{+1/2} \approx 11$. It is also found that the breakdown is not associated with the lodging of quasi-streamwise vortices inside the riblet grooves, or with the inapplicability of the Stokes hypothesis to the flow along the grooves, but with the appearance of quasi-two-dimensional spanwise vortices below $y^+ \approx 30$, with typical streamwise wavelengths $\lambda_x^+ \approx 150$. They are connected with a Kelvin–Helmholtz-like instability of the mean velocity profile, also found in flows over plant canopies and other surfaces with transpiration. A simplified stability model for the ribbed surface approximately accounts for the scaling of the viscous breakdown with A_g^+.

Keywords: riblets; drag reduction; roughness; Kelvin–Helmholtz

1. Introduction

Riblets are small surface protrusions aligned with the direction of flow, which confer an anisotropic roughness to a surface. They are one of the few techniques that have been successfully applied to the reduction of the skin friction in turbulent boundary layers, both in the laboratory and in full aerodynamic configurations.

Riblets of very different geometries have been tested in wind tunnels, demonstrating drag reductions of the order of 10 per cent over flat plates. Walsh & Lindemann [1] tested several shapes, including triangular, notched-peak, sinusoidal and U-shaped riblets, obtaining maximum drag reductions of 7–8% for riblet spacings of approximately 15 wall units. A fairly broad early review was that of Walsh [2], and more recent ones are those of Choi [3], who emphasizes the work of the ERCOFTAC drag reduction group, and Bushnell [4], which is oriented towards drag-reduction techniques for aircraft. In his review on turbulent flows over rough walls, Jiménez [5] viewed drag reduction by riblets as a transitional roughness effect.

*Author for correspondence (jimenez@torroja.dmt.upm.es).

One contribution of 15 to a Theme Issue 'Flow-control approaches to drag reduction in aerodynamics: progress and prospects'.

Riblet experiments have also been conducted in oil channels, which allow larger riblet dimensions and better control of the geometry, although typically at lower Reynolds numbers and shorter development lengths than wind tunnels. For example, Bechert *et al.* [6] conducted extensive tests on blade-shaped and trapezoidal-groove riblets, and proposed the latter as a compromise between optimum performance and practical fabrication and maintenance.

A recurrent theme of riblet research has been the motivation to study biological surfaces, which are often geometrically complex. Bruse *et al.* [7] conducted oil channel tests of shark-skin replicas, hairy surfaces and riblets with adjustable geometry, and Bechert *et al.* [8] reviewed the drag-reduction properties of biological surfaces and their replicas. More recently, Itoh *et al.* [9] tested the flow over seal fur, obtaining drag reductions of 12 per cent.

Off-design conditions have also been considered. We will discuss later the consequences of yaw and tip erosion, but we should mention here the effect of adverse pressure gradients, first reviewed by Walsh [2]. Although that condition is probably not the deciding factor in many practical applications, because the skin friction of adverse pressure gradient boundary layers tends to be low, pressure gradients of either sign are present over large areas of most practical configurations, and their effect on riblets remains uncertain. Walsh [2] found that riblet performance improved under adverse pressure gradients, but mentioned contradictory results by other authors, which he justified by the difficulty of using drag balances under those conditions. Coustols & Savill [10] summarized the results of several previous investigations, and concluded that the pressure gradients typically found over aircraft wings, whether adverse or favourable, had relatively little effect on the performance of riblets, while Debisschop & Nieuwstadt [11] tested riblets in a wind tunnel with dimensionless adverse pressure gradients an order of magnitude larger than those discussed in Walsh [2], and found that the maximum drag reduction of triangular riblets could increase roughly from 7 to 13 per cent.

Riblets have been used successfully to reduce the overall drag of aerofoils [12] and aircraft [13] with optimum riblet spacings of the order of 30–70 μm. Szodruch [14] reports on the flight tests of a commercial aeroplane (Airbus 320) with riblets over 70 per cent of its surface, and estimates an overall 2 per cent drag reduction, based on the fuel savings obtained. A summary of those tests, including maintenance and durability issues, can be found in Robert [15]. The discrepancy between the optimum laboratory performance and full configurations is probably to be expected from any method based on the reduction of skin friction. Not all the drag of an aircraft is friction [16], and much of the latter is distributed over three-dimensional or geometrically complex areas where drag control is difficult to optimize. Note that those limitations might not apply to configurations that are very different from commercial aircraft, such as gliders or other high-performance vehicles.

There is anecdotal evidence of the successful use of riblets in applications other than aircraft, particularly in sporting events in which cost and maintenance considerations are less important than in commercial aviation. The hulls of the USA challengers in the America's Cup 1987 and 2010 sailing competitions were fitted with riblets, which had been banned by the regulations in intervening years. Both challenges succeeded, although it is impossible to determine whether riblets

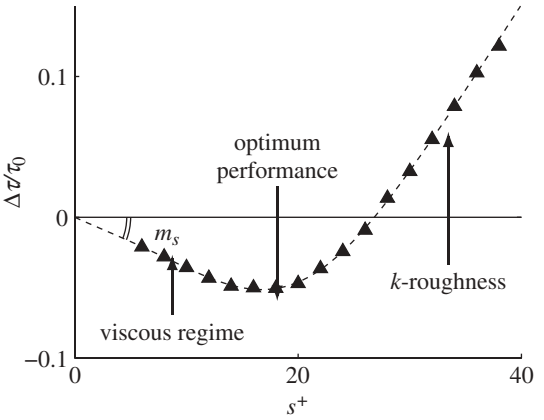

Figure 1. Definition of the drag-reduction regimes observed over triangular riblets with 60° tip angle, as a function of the peak-to-peak distance s^+. Adapted from Bechert *et al.* [6].

had any real role. Riblets were also used in the 1984 Olympic rowing events, but they were subsequently forbidden in official racing, together with all other devices that 'modify the properties of the boundary layer'.

The physical mechanism of the drag reduction by riblets has been investigated in detail, although some aspects remain controversial. In particular, mean and local velocity profiles and turbulent statistics within and above the riblet grooves have been reported for experiments in wind tunnels [17–19], water channels [20] and numerical experiments [21–26].

Walsh & Lindemann [1] showed that the Reynolds number dependence of the effect of riblets on the skin friction could be expressed in large part in terms of the riblet dimensions expressed in wall units, $L^+ = Lu_\tau/\nu$, where ν is the kinematic viscosity and $u_\tau = \tau^{1/2}$ is the friction velocity defined in terms of the skin friction τ, where we have assumed unit fluid density for simplicity. The same will be done throughout the paper. A popular measure of the riblet size L is the groove spacing, s, but other dimensions, such as the depth h, have also been used. We will propose below an alternative that collapses the experiments better, and that has some theoretical support. Figure 1 shows a typical curve of drag reduction as a function of the spacing, in which different drag regimes can be defined according to how the drag depends on s^+. In the viscous regime, formally $s^+ \ll 1$ but in practice $s^+ \lesssim 10$–15, the contribution of the nonlinear terms to the flow within and in the immediate neighbourhood of the riblet grooves is negligible and, if τ_0 is the skin friction for the smooth wall, the drag reduction $DR = -\Delta\tau/\tau_0$ is proportional to s^+. The viscous regime breaks down near $s^+ = s^+_{\mathrm{opt}}$, the optimum spacing for which drag reduction is maximum, and, eventually, the reduction becomes a drag increase, adopting a typical k-roughness behaviour [5]. The parameters that determine the optimum performance of a given riblet are its optimum size and the slope of the drag curve in the viscous regime. Both depend on the geometry, but the qualitative drag curve is always as just described.

This paper is organized as follows. Section 2 considers the suitability of the parameters traditionally used to scale the drag-reduction curves, and proposes an alternative. Section 3 reviews the viscous regime of drag reduction, including

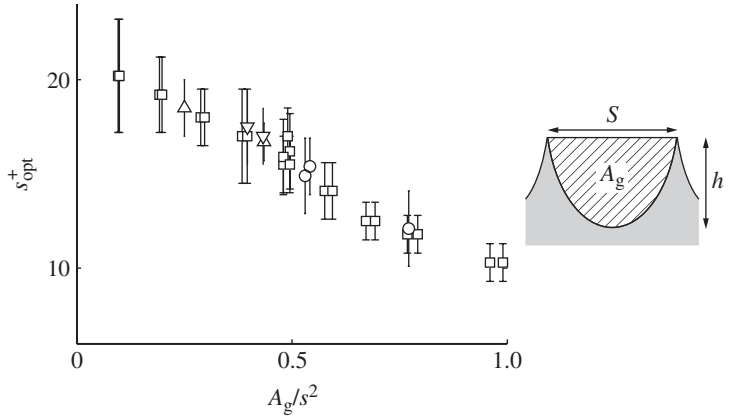

Figure 2. Riblet spacing for maximum drag reduction, as a function of the groove aspect ratio, A_g/s^2. Triangles, triangular riblets; inverted triangles, notched top and flat valley riblets; circles, scalloped semicircular grooves; squares, blade riblets [6]. Error bars have been estimated from the drag measurement errors given in the original reference.

the effects of yaw and tip rounding, and §4 centres on the range of optimum drag reduction, with particular emphasis on the reasons for the breakdown of the viscous regime, and on the linear stability of the flow. The conclusions are then summarized.

2. Scaling of the drag-reduction curves

We saw above that the drag reduction by riblets is a function of the riblet size expressed in wall units, and that it has become common to characterize that size by the spacing s^+. We now enquire whether some other choice of riblet dimensions describes experimental evidence better. Considering a generic length L, the drag behaviour in the viscous regime is characterized by the slope

$$m_L = -\left.\frac{\partial(\Delta\tau/\tau_0)}{\partial L^+}\right|_{L=0}, \tag{2.1}$$

so that $DR \approx m_L\, L^+$. We will see in §3 that this slope can usually be computed theoretically, but a successful parameter should also predict the location L^+_{opt} of the breakdown of the linear behaviour, and collapse as much as possible the experimental drag curves for $L \lesssim L_{opt}$. An approximation that has often been used is that $s^+_{opt} \approx 15$, but this quantity is a function of the riblet geometry. As an example, figure 2 shows the optimum spacing against the ratio of the groove cross section to the square of the spacing, A_g/s^2, for several riblet shapes. For a given spacing, higher values of A_g/s^2 imply deeper grooves, and, although s^+_{opt} is always in the range 10–20, it is clear from the figure that deeper grooves break down earlier, and that their maximum drag reduction is achieved for narrower riblets.

Using experimental results from Bechert *et al.* [6] for triangular, trapezoidal, blade and scalloped riblets, García-Mayoral & Jiménez [26] tested alternative scalings to find whether it was possible to express drag reduction in terms of a

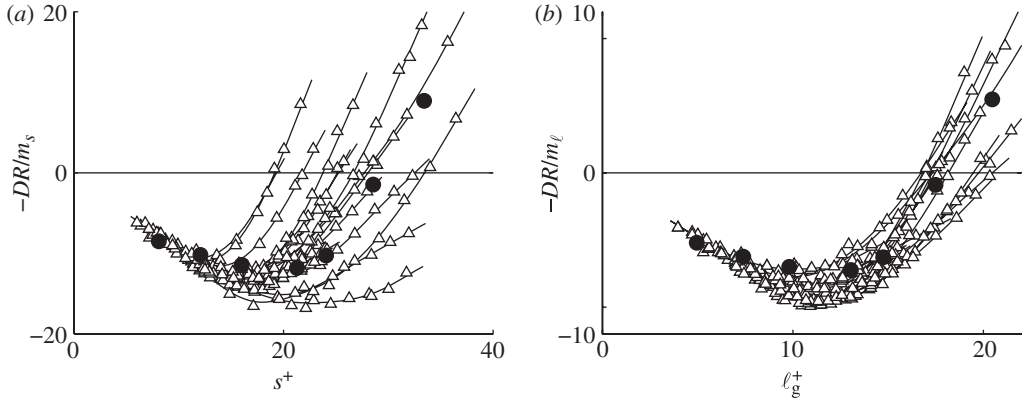

Figure 3. Drag-reduction curves of diverse riblets, reduced to a common viscous slope. Drag reduction (a) as a function of the spacing s^+ and (b) as a function of the square root of the groove cross section, ℓ_g^+. Open triangles, experimental results from Bechert *et al.* [6]; filled circles, direct numerical simulation results from García-Mayoral & Jiménez [26].

geometric parameter that captured both the influence of the riblet spacing and shape. The best results were achieved for the square root of the groove cross section, $\ell_g^+ = (A_g^+)^{1/2}$. The optimum values of s^+ or h^+ have scatters of the order of 40 per cent, while the optimum ℓ_g^+ only varies by approximately 10 per cent around $\ell_{g,opt}^+ \simeq 10.7 \pm 1.0$, for all the geometries reviewed.

Figure 3 compares experimental drag curves for a wide variety of riblet geometries, reduced with the appropriate viscous slope to compensate for the differences in viscous performance. The figure shows that there is good collapse of the data with ℓ_g^+, at least for $\ell_g^+ \lesssim 15$. For the different geometries portrayed, DR_{max} is roughly 83 per cent of the value that would result from extrapolating the linear viscous regime up to $\ell_{g,opt}^+$. The approximation

$$DR_{max} = 0.83\, m_\ell\, \ell_{g,opt}^+ \approx 8.9\, m_\ell, \tag{2.2}$$

using a fixed $\ell_{g,opt}^+ = 10.7$, is quite accurate for conventional riblets. That is tested in figure 4*a*, which compares experimental values of m_ℓ and DR_{max}. Even for riblets with depth-to-width ratios as low as 0.2, the error of the approximation (2.2) is below 20 per cent.

However, it should be stressed that, although ℓ_g^+ collapses the drag curves better than s^+ or h^+ for conventional geometries, there is no reason why it should do the same for unconventional configurations, such as the fibre riblets in Bruse *et al.* [7], the seal fur surface proposed by Itoh *et al.* [9] or the T-shaped riblets mentioned in Walsh [2]. Taking the latter as examples, the grooves become increasingly isolated from the overlying flow as the wall-parallel segments of the T-fences close into each other, but the groove area (or the groove spacing) changes little. For the limit of fully sealed grooves, the geometry would behave as a flat surface, and modifying ℓ_g^+ should have no performance impact. The scaling with ℓ_g^+ can only be considered as an empirical curve fit that works better than others for the experiments on existing geometries, but which should not be used

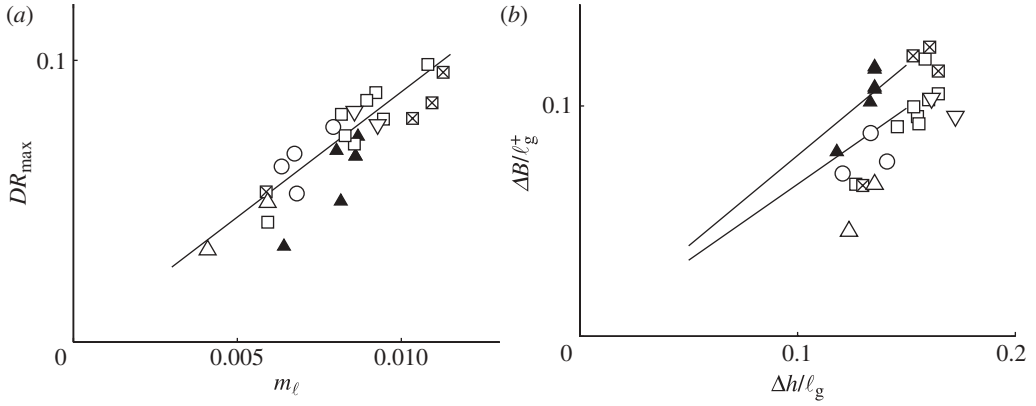

Figure 4. (*a*) Maximum drag reduction $DR_{\max}$ as a function of the experimental viscous slope m_ℓ. The solid line represents equation (2.2). (*b*) Experimental values of the viscous slope, as a function of the theoretical protrusion height. The two straight lines are $\mu_0 = 0.66$ and 0.785. In both (*a*) and (*b*), triangles, triangular riblets; inverted triangles, trapezoidal grooves; circles, scalloped grooves; squares, blades. Filled symbols are results from Walsh & Lindemann [2] and Walsh [1] and open ones from Bechert *et al.* [6].

uncritically for configurations that are very different from conventional ones. On the other hand, some theoretical justification for its use in conventional riblets is provided in §4.

3. The viscous regime

We now discuss the concept of protrusion height, which is generally considered to describe well the behaviour of riblets in the viscous regime. From here on, we will denote the streamwise, wall-normal and spanwise coordinates by x, y and z, respectively, and the corresponding velocity components by u, v and w.

There is a thin near-wall region in turbulent flows over smooth walls where viscous effects are dominant, nonlinear inertial effects can be neglected, and the mean velocity profile is linear. Its thickness is 5–10 wall units [27]. From the point of view of a small protrusion in this layer, the outer flow can be represented as a time-dependent, but otherwise uniform shear. Riblets destroy this uniformity near the wall but, if s^+ is small enough, the flow still behaves as a uniform shear for $y \gg h$. Because the equations of motion are locally linear, the riblets are uniform in the streamwise direction, and the shear varies only slowly with x when compared with riblet dimensions, the problem reduces to two uncoupled two-dimensional sub-problems in the z–y cross plane. The first one is the longitudinal flow of u, driven at $y^+ \gg 1$ by a streamwise shear

$$u \propto y - \Delta_u, \tag{3.1}$$

and the second one is the transverse flow of v and w, driven by

$$w \propto y - \Delta_w \quad \text{and} \quad v = 0. \tag{3.2}$$

Far from the wall, the effect of the riblets reduces to the virtual origins $\boldsymbol{\Delta}_u$ and $\boldsymbol{\Delta}_w$ [28]. Bechert & Bartenwerfer [29] had suggested that $\boldsymbol{\Delta}_u$ was the explanation of the drag reduction, essentially because it moved turbulence away from the wall, but Luchini *et al.* [30] noted that the important quantity was the offset $\Delta h = \Delta_w - \Delta_u$, the 'protrusion height', which is independent of any arbitrary reference wall position. Intuitively, if the cross-flow has a higher virtual origin than the longitudinal one ($\Delta h > 0$), the spanwise flow induced by the overlying streamwise vortices is impeded more severely than over a smooth wall. The streamwise vortices are displaced away from the wall, and the turbulent mixing of streamwise momentum is reduced. Since this mixing is responsible for the high local shear near the wall [31], its reduction results in a lower skin friction. The numerical calculation of Δh only involves the two stationary two-dimensional Stokes problems for $\boldsymbol{\Delta}_u$ and $\boldsymbol{\Delta}_w$, which are computationally much less intensive than the three-dimensional, time-dependent, turbulent flow over a ribbed wall.

The relation between protrusion height and drag is modified by the effect of the rest of the boundary layer velocity profile. The classical theory of wall turbulence is that surface manipulations only modify the intercept of the logarithmic velocity profile, while both the Kármán constant, $\kappa \approx 0.4$, and the wake function are unaffected [32]. The free-stream velocity, U_δ, can then be expressed as

$$U_\delta^+ = \left(\frac{2}{c_f}\right)^{1/2} = \kappa^{-1} \log \delta^+ + B, \tag{3.3}$$

where δ is a suitable flow thickness, δ^+ is the friction Reynolds number and B includes both the near-wall intercept and the contribution from the 'wake' component. The effect of a given ribbed surface would be to change B, which is equivalent to the 'roughness function' used to characterize rough surfaces [5]. For constant U_δ and small relative variations of the friction, it follows from equation (3.3) that

$$\frac{\Delta c_f}{c_{f0}} = \frac{\Delta \tau}{\tau_0} = -\frac{\Delta B}{(2c_{f0})^{-1/2} + (2\kappa)^{-1}}, \tag{3.4}$$

where the first term in the denominator is due to the change of u_τ in U_δ^+, and the second one comes from the corresponding change in δ^+. Comparison between riblets at different Reynolds numbers should be done in terms of ΔB, not of $\Delta\tau/\tau_0$, and the same is true when reducing experimental data to practical applications. The classical theory of wall turbulence suggests that, if the riblet size is much smaller than δ, which holds easily in the drag-reducing range, the effect of riblets should be confined to the near-wall layer, and that any change in B should only depend on the geometry of the riblets scaled in wall units. Note that equation (3.4) predicts that riblets lose effectiveness at high δ^+, such as in practical aerodynamic configurations, but only through the logarithmically slow decrease in c_{f0}.

Because of the linearity of the viscous regime, the change ΔB should be proportional to the protrusion height Δh^+,

$$\Delta B = \mu_0 \Delta h^+, \tag{3.5}$$

with a universal coefficient μ_0. That was tested by Jiménez [33], who performed direct simulations of channels at very low δ^+, in which the offset of the boundary conditions was modelled independently of the presence of actual riblets. He obtained $\mu_0 \approx 0.66$. A different argument by Bechert *et al.* [6], based on the uniform translation of the velocity profile, suggests $\mu_0 \approx 0.785$. Equation (3.5) is tested against experiments in figure 4*b*, but the experimental scatter is too large to distinguish between the two coefficients, or even to decide on the applicability of equation (3.5). At least some of the scatter is due to experimental artefacts. Wind tunnel and oil channel experiments are not strictly comparable, mostly because of the very different development lengths of the two set-ups, but also because of the different levels of geometric control, not always in the expected direction. For example, the open squares in figure 4 are blade riblets from Bechert *et al.* [6]. Those with crosses were mounted on a different base than those without them, and they agree better with the theory. Bechert noted the discrepancy, and repeated a few experiments after sealing the riblet base, increasing the drag reduction by about one-fifth. Similar caveats apply to the other riblets in the figure, including those that appear to agree with the theory.

However, if we believe the theoretical predictions in spite of the experimental ambiguities, equations (3.5) and (3.4) can be combined in a formula for the viscous drag-reduction slope m_ℓ that only depends on Stokes calculations,

$$m_\ell = \frac{\mu_0}{(2c_{f0})^{-1/2} + (2\kappa)^{-1}} \frac{\partial(\Delta h)}{\partial \ell_g}. \tag{3.6}$$

The results could then be used in the equivalent of figures 4*a* or 3*b* to predict the riblet performance, at least up to the limit of optimal drag reduction.

(*a*) *The effect of yaw*

The tools discussed above can be used to make useful predictions of the behaviour of riblets in off-design situations. A simple case is the effect of a misalignment angle θ between the riblets and the flow, which was first measured experimentally by Walsh [2]. He found that its effect on drag reduction was negligible up to $\theta = 15°$, which has been confirmed several times since then. The experiments also find that the drag reduction vanishes at $\theta = 25$–$35°$, and that the maximum drag increase occurs for $\theta = 90°$. A list of relevant references can be found in the paper by Koeltzsch *et al.* [34].

Consider now the viscous regime. Since the problem is linear, the longitudinal and transverse velocity with respect to the free stream can be projected into the frame of reference of the riblets, with the result that the offsets with respect to the flow are linear combinations of the offsets of perfectly aligned riblets, and that the protrusion height decays with the yaw as $\Delta h(\theta) = \cos(2\theta)\Delta h(0)$ [35]. That agrees qualitatively with the experiments mentioned above.

On the other hand, that simple dependence does not extend away from the viscous regime. Hage *et al.* [35] reported on the effect of yaw on riblets near the optimum spacing, and found a typically larger geometry-dependent degradation than in the viscous case, increasing strongly as s^+ exceeds the optimum value. Since the viscous breakdown is an indication of the effect of nonlinearity on the riblets, it is not surprising that the linear predictions do not apply in that limit.

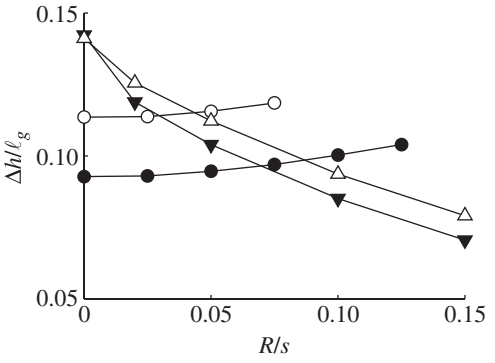

Figure 5. Protrusion height of rounded peak riblets, scaled with the characteristic length scale $\ell_g = (A_g)^{1/2}$ as a function of the peak radius of curvature. Filled inverted triangles, triangular riblet with tip angle 60°; open triangles, triangular riblet, 45°; open circles, blade riblet, $h/s = 0.5$ and thickness $t/s = 0.15$; filled circles, blade riblet, $h/s = 0.5$ and $t/s = 0.25$.

(*b*) *The impact of tip rounding*

Another effect that can be analysed using the results of the previous two sections is riblet erosion, which is a major concern for industrial applications. Walsh [37] measured drag reductions for triangular riblets with rounded peaks, finding a performance loss of up to 40 per cent for a tip radius $R \approx 0.08s$. He found no significant performance degradation from the rounding of the groove bottoms.

We can infer from the discussion in §2 that the details of the tip geometry should not affect significantly the viscous breakdown, because they barely modify the groove cross section. That is supported by the experiments of Bechert *et al.* [6], who tested blade and scalloped geometries in which only the tip thickness changed. The maximum drag reductions changed with the tip thickness, but not the optimum s^+, suggesting that the differences in performance were due to the changes in the slope of the drag-reduction curve in the viscous regime.

Viscous results for different geometries with tip rounding are presented in figure 5. The triangular riblets show a dramatic performance decrease, in agreement with Walsh [37], but the protrusion heights for flat-top blades, which perform worse for $R = 0$ than the sharp triangles, change little with tip rounding, and even increase slightly with growing radii. It is common knowledge [6,30] that sharper riblets have higher protrusion heights. Tip rounding reduces the sharpness of those configurations, and degrades their performance, but the rounding of the tips of initially blunt blades in a sense sharpens them, thus improving their performance. For practical applications in which erosion is an issue, it is probably preferable to use riblets that do not depend initially too much on the sharpness of their tips.

4. The breakdown of the viscous regime

In this section, we discuss the physical mechanism leading to the breakdown of the viscous regime. This is a key issue in riblet design, because we have seen that the optimum drag reduction is proportional to the riblet size at breakdown, and using larger riblets would lead to better optimum performance.

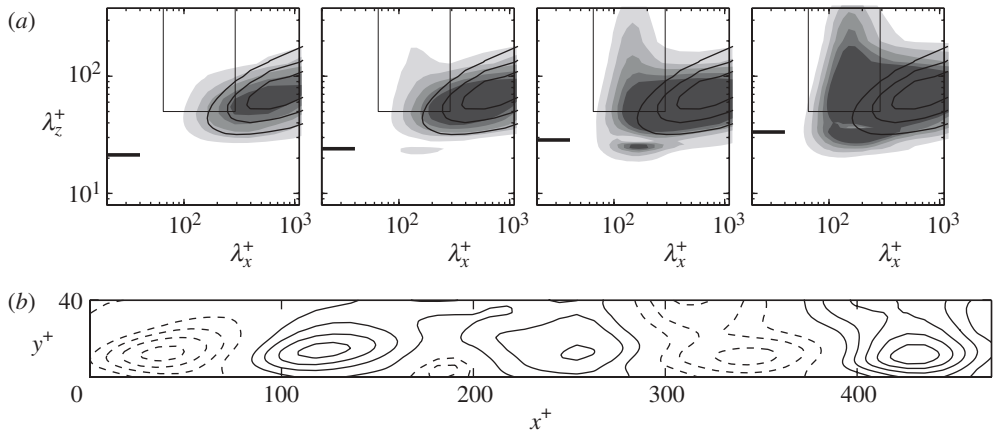

Figure 6. (*a*) Premultiplied two-dimensional cospectra of the Reynolds shear stress at $y^+ \approx 4$ above the riblet tips, for blade riblets of thickness $t/s = 0.25$, from García-Mayoral & Jiménez [26]. From left to right, $\ell_g^+ \approx 13$, 15, 17 and 20. The superimposed solid contour lines correspond to the smooth-wall case. The contour increments are $0.0035u_\tau^2$. The thick horizontal line to the left of each plot marks the riblet spacing, and the thin rectangle is the spectral region isolated in figure 7. (*b*) Detail near the wall of the instantaneous streamlines of the z-averaged perturbation u–v flow, for $\ell_g^+ \approx 17$, in a simulation box with $L_z^+ \approx 850$. The solid lines correspond to clockwise-rotating rollers, and the separation between streamlines is 1.3ν.

The theories proposed in the literature fall into two broad groups. The first one is that the effect of the riblets on the cross-flow loses effectiveness once they move beyond the Stokes regime. For example, Goldstein & Tuan [24] suggested that the deterioration is due to the generation of secondary streamwise vorticity over the riblets, because the unsteady cross-flow separates and sheds small-scale vortices that create extra dissipation. However, it is known that spanwise wall oscillations, which also presumably introduce unsteady streamwise vorticity, can decrease drag [38], and that spanwise boundary conditions that inhibit the creation of secondary wall vorticity can increase it [39], suggesting that the presence of extra vorticity near the wall need not be detrimental for drag reduction.

The second group of theories assumes that the observed optimum wavelength, $s^+ \approx 10$–20, is related to the scale of the turbulent structures in the wall region, such as in the observations by Choi *et al.* [21], Suzuki & Kasagi [20] and Lee & Lee [19], that the increase in drag coincides with the lodging of the quasi-streamwise vortices within the riblet grooves. However, all those observations are for $s^+ =$ 30–40, well past the optimum size.

García-Mayoral & Jiménez [26] recently documented a different scenario in a series of direct numerical simulation experiments with riblets spanning the full range of sizes from drag reduction to drag increase. They observed, for riblet sizes around the optimum, the formation of near-wall spanwise vortex rollers whose intensity grows rapidly with the riblet size. Those structures can be seen in the two-dimensional spectra of the flow variables, shown in figure 6*a* for the Reynolds shear stress $\tau = -\langle uv \rangle$, and their dimensions for different riblet sizes remain essentially constant in wall units. They have streamwise wavelengths $\lambda_x^+ \approx 150$, and only exist below $y^+ \approx 30$ when y^+ is referred to the plane of the riblet tips.

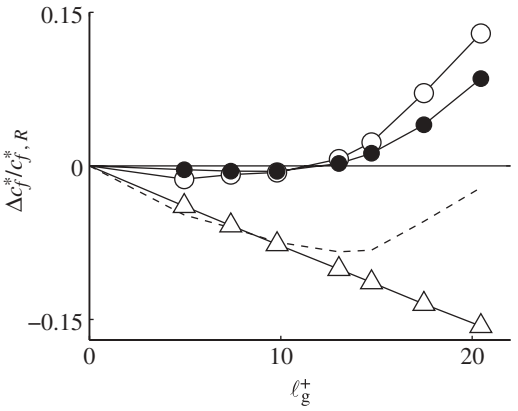

Figure 7. Break-up of the drag reduction curve, as defined in equation (4.1). Open triangles, slip term; open circles, full Reynolds stress term; filled circles, Reynolds stress term calculated only within the spectral region outlined in figure 6*a*; dashed line, full approximate drag reduction, $\Delta c_f^*/c_f^*$.

They are long in the spanwise direction, extending from $\lambda_z^+ \approx 50$ to the full channel width. An example can be seen in figure 6*b*, which shows instantaneous spanwise-averaged streamlines in the x–y plane. The rollers are centred at $y^+ \approx 10$–15, and penetrate slightly into the riblet grooves. The streamwise separation between rollers of the same sign is $\lambda_x^+ \approx 150$, in agreement with the spectra. Note that, since this figure is a spanwise average over a box with $L_z^+ \approx 850$, the aspect ratio of the surviving rollers is at least 10 with respect to x and 30 with respect to y, implying a quasi-two-dimensional phenomenon in an x–y plane.

Although, to our knowledge, those structures have not been reported before, they can be seen, in retrospect, in some of the visualizations of Goldstein *et al.* [23] and Chu & Karniadakis [22], and it is interesting that, even in conditions very different from ours, their streamwise wavelengths are also in the range $\lambda_x^+ = 100$–200.

The new structures account for most of the degradation of riblet performance with size. Consider two channels with identical half-width, δ, and centreline velocity U_δ, one of them with riblets (R), and the other without (S). Define an approximate wall friction, $u_*^2 = -(\partial_x P)\delta$, as the extrapolation of the total stress, $\tau(y) + \nu \partial_y U$, to $y = 0$, which is the plane of the riblet tips. Note that this is not the skin friction that should be used in the true friction coefficient of the ribbed channels, because it neglects the effect of the streamwise pressure gradient over the cross section of the grooves, but it has the same qualitative behaviour as the real one, and can be used for the present argument. That can be seen by comparing the dashed line in figure 7, which is the friction coefficient computed in this way, with the filled circles in figure 3*b*, which are the true friction coefficients for the same cases. A complete treatment of the following discussion can be found in García-Mayoral & Jiménez [26]. Integrating the mean momentum equation for the two channels and defining the approximate friction coefficient as $c_f^* = 2u_*^2/U_\delta^2$, it can be shown by integrating the momentum

equation between the planes of the riblet tips that the drag change owing to the riblets is

$$\frac{\Delta c_f^*}{c_{f,\mathrm{R}}^*} = -\frac{U_{0,\mathrm{R}}}{U_{\delta,\mathrm{R}}} + \frac{1}{U_{\delta,\mathrm{R}}^*}\int_0^{\delta_\mathrm{R}^*} (\tau_\mathrm{R}^* - \tau_\mathrm{S}^*)\,\mathrm{d}y_\mathrm{R}^*, \tag{4.1}$$

where quantities with asterisks are normalized with their own u_*, and subscripts refer to the channel type. The two terms on the right-hand side are plotted independently in figure 7. The first one is the slip velocity at the plane of the riblet tips, owing to the presence of the grooves, and always reduces skin friction. That is essentially the mechanism of drag reduction in the viscous regime, and it is interesting that it remains proportional to the riblet size across the figure, even after the drag starts to increase. The slip velocity in figure 7 follows almost exactly the predictions of the longitudinal Stokes problem (3.1), even for the larger riblets, showing that the deterioration of the drag is not due to the breakdown of the viscous hypothesis within the groove. It turns out that the velocities within the groove are small enough that their Reynolds numbers remain small.

The deterioration is due to the extra Reynolds stress in the second term of equation (4.1), whose integrand is small everywhere except near $y = 0$, because the two stresses have been scaled to approximately coincide far from the wall. Moreover, the figure includes, in open symbols, the integral of the full Reynolds stress, and, in filled ones, the result of considering only the cospectrum in the spectral region of the new structures, $65 \leq \lambda_x^+ \leq 290$, $\lambda_z^+ \geq 50$ and $y^+ \lesssim 35$. It is clear that the stresses responsible for the drag degradation are those of the new spanwise structures.

The formation of structures perpendicular, rather than parallel, to the riblets may seem surprising, but it is not completely unexpected. Similar spanwise rollers have been reported over vegetable canopies [40,41], and over permeable [42] and porous walls [43]. The length scale of the structures varies depending on the particular problem, but, although few quantitative analyses exist in the literature [42,44], the phenomenon has always been attributed to a Kelvin–Helmholtz-like instability. In essence, the mean profile of a boundary layer almost has an inflection point at the wall, and the reason that it remains inviscidly stable is that the impermeability condition, $v = 0$, precludes the antisymmetric unstable eigenfunctions characteristic of Kelvin–Helmholtz. Once any modification of the wall allows local transpiration, the inflection-point instability reappears.

García-Mayoral & Jiménez [26] adapted that general idea to ribbed surfaces. The conceptual model is that the longitudinal Stokes flow along the grooves is driven by the pressure variation of the overlying turbulent flow, and that the resulting longitudinal variations of the velocity within the grooves create a wall-normal transpiration that acts as a boundary condition for an inviscid Rayleigh equation for linearized perturbations around the mean velocity profile in $y > 0$. The boundary condition has the form

$$(\partial_t + U\partial_x)\partial_y v = U'\partial_x v \mp \frac{\nu v}{L_\mathrm{w}^3}, \tag{4.2}$$

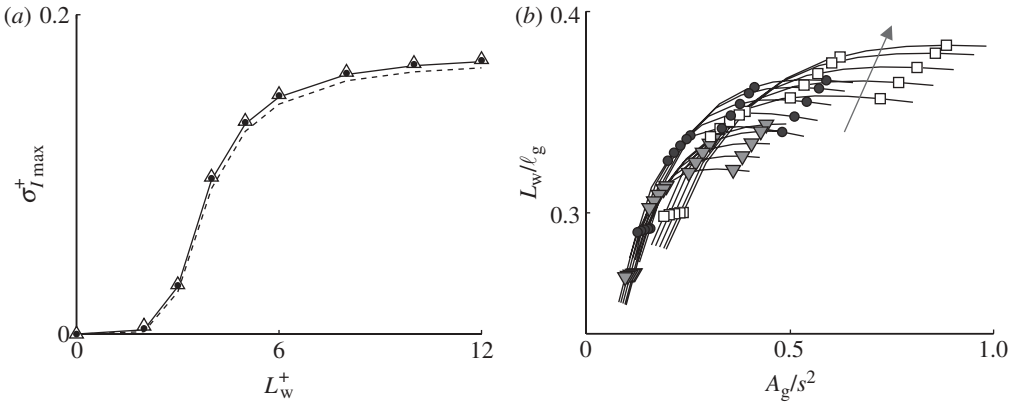

Figure 8. (*a*) Maximum growth rate of the transpiration instability in turbulent channels, as a function of the parameter L_w^+ defined in equation (4.3). Dashed line, $\delta^+ = 185$; solid line, 550; filled circles, 950; open triangles, 2000. (*b*) Ratio L_w/ℓ_g, for conventional riblets. Filled inverted triangles, triangular riblets; filled circles, scalloped grooves; open squares, blade riblets. The solid lines connect riblets of the same type with equal tip width, which decreases in the direction of the arrow.

where the two signs of the last term apply, respectively, to the upper and lower walls and U' is the gradient of the mean velocity at the wall. The new parameter L_w can be interpreted as a length scale for the groove cross section, and is defined as

$$L_w^3 = s^{-1} \iint_{A_g} f \,\mathrm{d}y \,\mathrm{d}z, \tag{4.3}$$

where f is the velocity owing to a normalized pressure gradient along the groove, $\partial_x P = -\nu$, and satisfies $\nabla^2 f = -1$. It has dimensions of length squared and depends only on the groove geometry. The flow is unstable for all $L_w > 0$, but figure 8*a* shows that the instability only becomes significant for $L_w^+ \gtrsim 4$, essentially independently of the Reynolds number of the flow above the wall.

The values of L_w for several conventional riblet shapes are compiled in figure 8*b*, which shows that $L_w \approx 0.35\,\ell_g$ for groove aspect ratios larger than $A_g/s^2 \approx 0.4$. Together with the stability threshold just mentioned, this result suggests that the flow becomes unstable above $\ell_g^+ \approx 11$, giving some theoretical support to the scaling of the drag curves found empirically in §2.

5. Conclusions

We have reviewed the regimes for drag reduction in ribbed surfaces, with particular emphasis on the practical information that can be extracted from the viscous regime, and on the conditions under which that regime breaks down. We have shown that the existing experiments for the location of the breakdown collapse better with a new length scale, $\ell_g^+ = A_g^{+1/2}$, based on the groove area, than with more classical choices such as the riblet spacing or depth.

The best estimate for optimum drag reduction is $\ell_g^+ \simeq 10.7$, which, together with the drag slope in the viscous limit, can be used to predict riblet performance within 20 per cent. We have shown that this probably predicts the effect of tip erosion, which, somewhat surprisingly, is not always deleterious, but that the effect of yaw for optimized riblets is only qualitatively predicted by the viscous regime.

Using direct simulations of ribbed channels spanning the range from viscous drag reduction to drag increase, we have shown that the degradation for large riblets of the linear regime of drag reduction is not connected with the breakdown of the Stokes behaviour of the longitudinal velocity along the riblet grooves. Even when the drag is already increasing, the slip velocity at the plane of the riblet tips remains proportional to the riblet size. The extra drag comes from a system of spanwise vortices below $y^+ \approx 30$, with dimensions that scale in wall units, independently of the riblet size. We have connected those rollers to a Kelvin–Helmholtz-like instability common to other systems with surface transpiration, such as canopies, and permeable and porous surfaces, and we have described a model for ribbed surfaces that provides some theoretical justification for the experimental scaling of the breakdown with the groove area.

This work was supported in part by the CICYT grant TRA2009-11498, and by the sixth framework AVERT programme of the European Commission, AST5-CT-2006-030914. R.G.-M. was supported by an FPI fellowship from the Spanish Ministry of Education and Science.

References

1 Walsh, M. J. & Lindemann, A. M. 1984 Optimization and application of riblets for turbulent drag reduction. AIAA paper 84-0347.
2 Walsh, M. J. 1990 Riblets. In *Viscous drag reduction in boundary layers* (eds D. M. Bushnell & J. N. Hefner), pp. 203–261. New York, NY: AIAA.
3 Choi, K.-S. 2000 European drag-reduction research—recent developments and current status. *Fluid Dyn. Res.* **26**, 325–335. (doi:10.1016/S0169-5983(99)00030-1)
4 Bushnell, D. M. 2003 Aircraft drag reduction—a review. *Proc. Inst. Mech. Eng.* **217**, 1–18. (doi:10.1243/095441003763031789)
5 Jiménez, J. 2004 Turbulent flows over rough walls. *Annu. Rev. Fluid Mech.* **36**, 173–196. (doi:10.1146/annurev.fluid.36.050802.122103)
6 Bechert, D. W., Bruse, M., Hage, W., der Hoeven, J. G. T. V. & Hoppe, G. 1997 Experiments on drag-reducing surfaces and their optimization with adjustable geometry. *J. Fluid Mech.* **338**, 59–87. (doi:10.1017/S0022112096004673)
7 Bruse, M., Bechert, D. W., der Hoeven, J. G. T. V., Hage, W. & Hoppe, G. 1993 Experiments with conventional and with novel adjustable drag-reducing surfaces. In *Near-wall turbulent flows* (eds R. M. C. So, C. G. Speziale & B. E. Launder), pp. 719–738. Amsterdam, The Netherlands: Elsevier.
8 Bechert, D. W., Bruse, M., Hage, W. & Meyer, R. 1997 Biological surfaces and their technological application—laboratory and flight experiments on drag reduction and separation control. AIAA paper 97-1960.
9 Itoh, M., Tamano, S., Iguchi, R., Yokota, K., Akino, N., Hino, R. & Kubo, S. 2006 Turbulent drag reduction by the seal fur surface. *Phys. Fluids* **18**, 065102. (doi:10.1063/1.2204849)
10 Coustols, E. & Savill, A. M. 1992 Turbulent skin-friction drag reduction by active and passive means: part I. In *Skin friction drag reduction*. AGARD report 786, pp. 8.1–8.53. Neuilly-sur-Seine, France: AGARD.
11 Debisschop, J. R. & Nieuwstadt, F. T. M. 1996 Turbulent boundary layer in an adverse pressure gradient: effectiveness of riblets. *AIAA J.* **34**, 932–937. (doi:10.2514/3.13170)

12 Lee, S.-J. & Jang, Y.-G. 2005 Control of flow around a NACA 0012 airfoil with a micro-riblet film. *J. Fluids Struct.* **20**, 659–672. (doi:10.1016/j.jfluidstructs.2005.03.003)
13 Viswanath, P. R. 2002 Aircraft viscous drag reduction using riblets. *Prog. Aerosp. Sci.* **38**, 571–600. (doi:10.1016/S0376-0421(02)00048-9)
14 Szodruch, J. 1991 Viscous drag reduction on transport aircraft. AIAA paper 91-0685.
15 Robert, J. F. 1992 Drag reduction: an industrial challenge. In *Skin friction drag reduction*. AGARD report 786, pp. 2.1–2.15. Neuilly-sur-Seine, France: AGARD.
16 Roskam, J. 1987 *Airplane design. Part VI: preliminary calculation of aerodynamic, thrust and power characteristics*. Ottawa, KS: Roskam Aviation and Engineering Corporation.
17 Vukoslavcevic, P., Wallace, J. M. & Balint, J.-L. 1992 Viscous drag reduction using streamwise aligned riblets. *AIAA J.* **30**, 1119–1122. (doi:10.2514/3.11035)
18 Park, S.-R. & Wallace, J. M. 1994 Flow alteration and drag reduction by riblets in a turbulent boundary layer. *AIAA J.* **32**, 31–38. (doi:10.2514/3.11947)
19 Lee, S.-J. & Lee, S.-H. 2001 Flow field analysis of a turbulent boundary layer over a riblet surface. *Exp. Fluids* **30**, 153–166. (doi:10.1007/s003480000150)
20 Suzuki, Y. & Kasagi, N. 1994 Turbulent drag reduction mechanism above a riblet surface. *AIAA J.* **32**, 1781–1790. (doi:10.2514/3.12174)
21 Choi, H., Moin, P. & Kim, J. 1993 Direct numerical simulation of turbulent flow over riblets. *J. Fluid Mech.* **255**, 503–539. (doi:10.1017/S0022112093002575)
22 Chu, D. C. & Karniadakis, G. E. M. 1993 A direct numerical simulation of laminar and turbulent flow over riblet-mounted surfaces. *J. Fluid Mech.* **250**, 1–42. (doi:10.1017/S0022112093001363)
23 Goldstein, D. B., Handler, R. & Sirovich, L. 1995 Direct numerical simulation of turbulent flow over a modeled riblet covered surface. *J. Fluid Mech.* **302**, 333–376. (doi:10.1017/S0022112095004125)
24 Goldstein, D. B. & Tuan, T. C. 1998 Secondary flow induced by riblets. *J. Fluid Mech.* **363**, 115–151. (doi:10.1017/S0022112098008921)
25 El-Samni, O. A., Chun, H. H. & Yoon, H. S. 2007 Drag reduction of turbulent flow over thin rectangular riblets. *Int. J. Eng. Sci.* **45**, 436–454. (doi:10.1016/j.ijengsci.2007.03.002)
26 García-Mayoral, R. & Jiménez, J. Submitted. Hydrodynamic stability and the breakdown of the viscous regime over riblets.
27 Tennekes, H. & Lumley, J. L. 1972 *A first course in turbulence*. Cambridge, MA: MIT Press.
28 Luchini, P. 1995 Asymptotic analysis of laminar boundary-layer flow over finely grooved surfaces. *Eur. J. Mech. B/Fluids* **14**, 169–195.
29 Bechert, D. W. & Bartenwerfer, M. 1989 The viscous flow on surfaces with longitudinal ribs. *J. Fluid Mech.* **206**, 105–129. (doi:10.1017/S0022112089002247)
30 Luchini, P., Manzo, F. & Pozzi, A. 1991 Resistance of a grooved surface to parallel flow and cross-flow. *J. Fluid Mech.* **228**, 87–109. (doi:10.1017/S0022112091002641)
31 Orlandi, P. & Jiménez, J. 1994 On the generation of turbulent wall friction. *Phys. Fluids* **6**, 634–641. (doi:10.1063/1.868303)
32 Clauser, F. 1956 The turbulent boundary layer. *Adv. Appl. Mech.* **4**, 1–51. (doi:10.1016/S0065-2156(08)70370-3)
33 Jiménez, J. 1994 On the structure and control of near wall turbulence. *Phys. Fluids* **6**, 944–953. (doi:10.1063/1.868327)
34 Koeltzsch, K., Dinkelacker, A. & Grundmann, R. 2002 Flow over convergent and divergent wall riblets. *Exp. Fluids* **33**, 346–350. (doi:10.1007/s00348-002-0446-3)
35 García-Mayoral, R. & Jiménez, J. 2007 On the effect of riblet geometry on drag reduction. Technical report ETSIA/MF-072, School of Aeronautics, Universidad Politécnica de Madrid.
36 Hage, W., Bechert, D. W. & Bruse, M. 2000 Yaw angle effects on optimized riblets. In *Proc. CEAS/DragNet European Drag Reduction Conf.* (ed. P. Thiede), pp. 278–285. Berlin, Germany: Springer.
37 Walsh, M. J. 1990 Effect of detailed surface geometry on riblet drag reduction performance. *J. Aircr.* **27**, 572–573. (doi:10.2514/3.25323)
38 Jung, W., Mangiavacchi, N. & Akhavan, R. 1992 Supression of turbulence in wall-bounded flows by high-frequency spanwise oscillations. *Phys. Fluids A* **4**, 1605–1607. (doi:10.1063/1.858381)

39 Jiménez, J. & Pinelli, A. 1999 The autonomous cycle of near wall turbulence. *J. Fluid Mech.* **389**, 335–359. (doi:10.1017/S0022112099005066)
40 Raupach, M. R., Finnigan, J. & Brunet, Y. 1996 Coherent eddies and turbulence in vegetation canopies: the mixing-layer analogy. *Bound. Layer Meteorol.* **78**, 351–382. (doi:10.1007/BF00120941)
41 Finnigan, J. 2000 Turbulence in plant canopies. *Annu. Rev. Fluid Mech.* **32**, 519–571. (doi:10.1146/annurev.fluid.32.1.519)
42 Jiménez, J., Uhlman, M., Pinelli, A. & Kawahara, G. 2001 Turbulent shear flow over active and passive porous surfaces. *J. Fluid Mech.* **442**, 89–117. (doi:10.1017/S0022112001004888)
43 Breugem, W. P., Boersma, B. J. & Uittenbogaard, R. E. 2006 The influence of wall permeability on turbulent channel flow. *J. Fluid Mech.* **562**, 35–72. (doi:10.1017/S0022112006000887)
44 Py, C., de Langre, E. & Moulia, B. 2006 A frequency lock-in mechanism in the interaction between wind and crop canopies. *J. Fluid Mech.* **568**, 425–449. (doi:10.1017/S0022112006002667)